



ELSEVIER

Materials Science and Engineering B101 (2003) 1–8

**MATERIALS
SCIENCE &
ENGINEERING
B**

www.elsevier.com/locate/mseb

Precision placement of heteroepitaxial semiconductor quantum dots

R. Hull^{a,*}, J.L. Gray^a, M. Kammler^{a,e}, T. Vandervelde^b, T. Kobayashi^c, P. Kumar^c,
T. Pernell^c, J.C. Bean^c, J.A. Floro^d, F.M. Ross^e

^a Department of Materials Science, University of Virginia, 116 Engineers Way, Charlottesville, VA 22904, USA

^b Department of Physics, University of Virginia, 382 McCormick Road, Charlottesville, VA 22904, USA

^c Department of Electrical and Computer Engineering, University of Virginia, 315 McCormick Road, Charlottesville, VA 22904, USA

^d Sandia National Laboratories, Albuquerque, NM 87185-1415, USA

^e IBM Thomas J. Watson Research Center, P.O. Box 218, Yorktown Heights, NY 10598, USA

Abstract

We describe two new approaches to the patterning of Si(1 0 0) surfaces for controlled nucleation of heteroepitaxial Ge semiconductor clusters. In the first method, a Ga⁺-focused ion beam in situ to the growth chamber is used to create local regions of enhanced Ga⁺ concentration and surface topography. It is shown that at low ion doses ($\sim 10^{14}$ cm⁻²), implanted Ga causes local nucleation of Ge clusters upon the implanted region. At higher doses ($\geq 10^{15}$ cm⁻²), a complex surface topography localizes nucleation of Ge clusters. This approach can be used to seed complex patterns of Ge clusters with diameters of tens of nanometers and positional accuracy of sub-100 nm. The second method employs self-assembly of complex strain-stabilized “quantum quadruplet” and “quantum fortress” structures, whereby cooperative island nucleation around shallow strain-relieving pits is identified during Ge_xSi_{1-x}/Si(1 0 0) heteroepitaxy. These configurations are kinetically limited structures that exist over a range of compositions, growth temperatures, and growth rates, but which are destabilized by strain relaxation (e.g. by the introduction of misfit dislocations) and by growth conditions which provide high adatom surface mobilities. Both methods have broad potential application to nanoelectronic device architectures.

© 2003 Elsevier Science B.V. All rights reserved.

Keywords: Strained layer epitaxy; Strain relaxation; Quantum fortress; Molecular beam epitaxy; Controlled nucleation

1. Introduction

It has long been recognized that during heteroepitaxial semiconductor growth of materials with different lattice parameters, strain may drive surface roughening or cluster formation as the epitaxial film grows. Further, the interactions between cluster strain fields can drive organization of such clusters into a single spatial frequency, particularly in multilayered structures (e.g. [1,2]). Such clusters can act as individual quantum entities for electron transport, allowing new potential nanoelectronic architectures, which generally require greater control of cluster positioning than ordering into a single spatial frequency. An example is the concept of quantum cellular automata (QCA) [3] where

additional electronic charges placed on an array of four quantum dots at the corners of a square assume bistable ground states according to electron occupation of the two pairs of opposite corners. This mimics the two states of digital logic and logic gates, and more complex circuits have been proposed based upon this phenomenon [3]. Power delay products and packing densities for such architectures can in principle be many orders of magnitude higher than in conventional Si MOSFET circuits. Initial experimental proofs of concept have been fabricated [4] using Al/Al₂O₃ tunnel junctions, but the highest operating temperatures reported to date have been of order 1 K, due to the low energy difference between the bistable states at dimensions accessible using conventional lithography techniques. The ability to pattern semiconductor cluster arrays of the necessary complexity and dimensions may allow higher temperature operation to be explored. Several approaches have been adopted to enable the required “programmability” of semiconductor surfaces prior to subsequent hetero-

* Corresponding author. Tel.: +1-804-982-5658; fax: +1-804-982-5660.

E-mail address: hull@virginia.edu (R. Hull).

epitaxial deposition, including selective growth within patterned ultra-thin SiO₂ masks [5], strain relaxation fields at the edge of topographical features (e.g. [6,7]), nano-imprinting techniques [8], and buried stress fields from oxygen implantation [9]. In this paper, we describe recent progress with two new approaches for patterned formation of Ge clusters on Si(1 0 0): in situ substrate patterning with a Ga⁺-focused ion beam (FIB), and spontaneous self-assembly of quantum dot quadruplets around shallow pits as a kinetically limited strain relief mechanism.

2. Strain relaxation modes in lattice-mismatched semiconductor heteroepitaxy

Heteroepitaxial semiconductor structures have been central to a broad range of fundamental advances in our understanding of the properties of matter, and are critical to the operation of multiple classes of electronic and optoelectronic devices. The development of crystal growth techniques such as molecular beam epitaxy (MBE) and chemical vapor deposition (CVD) has enabled such heterostructures to be grown with atomic-scale precision. However, there is a relatively limited amount of material combinations that can be grown with closely matched lattice parameters (particularly considering the relatively small set of semiconductor materials that can be successfully grown as high-quality single-crystal substrates). This range of available material combinations may be increased by extending to components with significantly different lattice parameters. This induces very large strains and stresses in the epitaxial films that can relax through a set of mechanisms, the most important of which at practical crystal growth and processing temperatures are elastic distortion of the epilayer, injection of interfacial misfit dislocations, and roughening of the epilayer surface.

In the first of these mechanisms, lattice mismatch strain is accommodated by a tetragonal distortion of the unit cell in the epitaxial layer, whereby the in-plane layer lattice parameter is forced to that of the substrate, and the out of plane lattice parameter distorts according to the Poisson effect (i.e. for the case of compressively strained Ge_xSi_{1-x} films on Si, the tetragonal distortion is outwards along the interfacial normal). For a lattice parameter difference of 1% (i.e. a biaxial strain of 0.01) and elastic constants typical to diamond cubic and zinc blende semiconductors, this gives rise to lattice mismatch stresses of the order 1–2 GPa. Such enormous stresses can be supported only in the limits of very thin films and low growth temperatures.

In the second of these mechanisms, interfacial misfit dislocations allow the epitaxial layer to relax towards its free lattice parameter. A critical epitaxial layer thickness [10] exists above which misfit dislocations are energeti-

cally favored in the film. Above this critical thickness, the strain energy relaxed in the film compensates the additional self-energy term associated with the dislocation strain field and core. The magnitude of the critical thickness can be predicted by equilibrium models based upon simple descriptions of the lattice mismatch-induced biaxial stress and the misfit dislocation line tension [10]. Experimental measurements confirm equilibrium predictions in the limit of very high growth or annealing temperatures (≥ 900 °C) [11,12], but at a lower growth temperature of 550 °C Ge_xSi_{1-x}/Si(1 0 0) heterostructures may be grown to epilayer thicknesses substantially beyond those predicted by equilibrium theory before significant misfit dislocation densities are observed [13]. This is a manifestation of metastability, whereby activation barriers associated with the nucleation and propagation of misfit dislocations greatly kinetically limit the rate of evolution of the interfacial misfit dislocation array at lower temperatures [14].

It is the third strain relaxation mechanism that is most relevant to this paper. Surface roughening allows interatomic bonds near the surface to relax towards distributions of angles and lengths of lower net energy. For compressively strained Ge_xSi_{1-x} epitaxial layers on Si, this produces regions of dilation of the surface lattice parameter (with respect to a uniform planar film) at the waveform peaks and compression at the waveform troughs. The resultant surface field may then induce compositional segregation on the growing epitaxial surface, e.g. in the Ge_xSi_{1-x}/Si system, Ge atoms would be expected to preferentially incorporate at the waveform peaks, where its larger bond length is more easily accommodated, and Si at the troughs.

The development of surface morphology requires sufficient adatom diffusion of the deposited species on the growth surface. Thus, the tendency for development of surface morphology increases with increasing growth temperature and decreasing growth rate as well as increasing epilayer strain. The evolution of surface morphology in the Ge/Si(1 0 0) system has been extensively studied. At growth temperatures greater than 500 °C (with a secondary dependence also on the growth rate), this system follows the Stranski–Krastanov mode, where a thin planar wetting layer of a few monolayers of Ge first forms, and then coherent (i.e. dislocation-free) islands form upon the wetting layer [15]. Depending upon the growth conditions, these coherent islands first adopt a characteristic “hut cluster” morphology with {5 1 0} sidewalls [16]. As deposition continues and individual islands grow, they next form coherent “dome morphologies”, initially with dominant {3 1 1} facets but then evolving into more complex surface facets, and finally the domes dislocate [17–19]. For Ge_xSi_{1-x} alloys on Si(1 0 0), the epilayer surface exhibits a similar set of transitions [20], provided the growth temperature (e.g. ≥ 700 °C for $x = 0.2$) is high

enough to allow sufficient surface diffusion of adatoms. The length scales for the transitions also increase according to scaling factors ε^{-1} to ε^{-2} [20–22], where ε is the lattice mismatch strain between epitaxial layer and substrate. Lower growth temperatures can lead to markedly different morphologies, as will be demonstrated by the kinetically limited quantum quadruplet/quantum fortress structures described later in this paper.

3. Experimental

For the experiments described in Section 4, FIB patterning, implant annealing, and CVD were performed in situ to a modified Hitachi ultra-high vacuum (base pressure: 2×10^{-10} Torr) transmission electron microscope (UHV-TEM) [23]. An integrated gas handling system permits the injection of disilane, digermane, and oxygen into the objective pole-piece area. This allows direct TEM observation of CVD growth process onto a resistively heated sample in real-time. The FIB source is connected under UHV to an adjacent preparation chamber. It is a commercially available two-lens gun [24] operated for this work at 25 keV and an ion beam current of 10 pA. The realized beam diameter (limited by electrical and mechanical noises in our environment) at this current is of order 80 nm.

Atomically clean, electron-transparent samples are prepared using a detailed procedure described elsewhere [25]. In brief, 100 μm thick Si samples were thinned using standard etching and electronic-grade cleaning techniques. After sample degassing for 12 h at 300 °C in the microscope load lock chamber, the native oxide was removed by repeated flashing of the sample to a temperature ~ 1250 °C. The cleaned sample was then transferred into the objective lens pole-piece and further thinned to electron transparency using in situ oxygen etching. Sample temperatures were estimated by extrapolation of heating currents calibrated to optical pyrometer readings in the range 750–1250 °C. Previously, we have demonstrated similar temperature calibrations in this instrument that were accurate to within 20–30 °C by direct observation of the Si(1 1 1) $1 \times 1 \leftrightarrow 7 \times 7$ surface transition in electron-transparent regions [26].

In the experiments described in Section 5, $\text{Ge}_x\text{Si}_{1-x}$ films were grown using MBE on (1 0 0) Si substrates using a custom-built chamber at Sandia National Laboratories [27,28] and a VG 90 double chamber system at the University of Virginia. For samples grown in the Sandia system, 300 μm thick substrates were chemically cleaned and oxidized using a modified Shiraki procedure [29] before being loaded into the growth chamber. The resulting surface oxide was desorbed at a temperature of 820 °C, and a 1000 Å Si buffer layer was then grown at 750 °C. After buffer

growth, the substrate temperature was lowered to the $\text{Ge}_x\text{Si}_{1-x}$ growth temperature (usually 550 °C for the results described herein). For many of the structures described here, a substantial pause (of order 1 h) then followed to enable temperature equilibration for real-time wafer curvature analysis of epilayer stress using an ultra-sensitive multibeam optical stress sensor (MOSS) technique [20,27,28]. However, we have established that subsequent growth morphologies are not significantly affected by this pause, both by control experiments on the Sandia system and by standard configuration experiments on the UVa system that do not employ this pause. Following temperature equilibration, a further 5 nm of Si buffer was grown followed by $\text{Ge}_{0.3}\text{Si}_{0.7}$ alloy growth at the same temperature. The base pressure in the chamber prior to growth was typically 2×10^{-10} Torr. The growth surface morphology was monitored using reflection high-energy electron diffraction (RHEED).

For samples grown in the UVa system, a modified “Piranha clean” procedure [30] was used to clean and hydrogen passivate the substrates before they were loaded into the growth chamber. The resulting hydrogen-terminated layer, along with any surface oxide, was desorbed at a temperature of 775 °C. A 1000 Å Si buffer layer was then grown starting at 775 °C. Near the end of the buffer growth, the substrate temperature was progressively lowered to the $\text{Ge}_x\text{Si}_{1-x}$ growth temperature, 550 °C. This allows for immediate growth of the epilayer, thereby eliminating any chance of contamination buildup. The base pressure in the chamber prior to growth was typically 5×10^{-10} Torr.

The surface morphology of as-grown films was characterized ex situ using contact-mode atomic force microscopy (AFM) using Park Scientific Autoprobe and Digital Instruments Nanoscope III instruments. Selected samples were also studied by TEM using both plan view and cross-sectional modes on a JEOL 2000 FX TEM operated at 200 kV.

4. Nucleation site patterning using FIB

Fig. 1 shows in situ TEM images ($\langle 2 2 0 \rangle$ g, 3g weak beam) of patterns created by in situ FIB sputtering in UHV-CVD-TEM. All patterns shown in this figure were created with a 10 pA Ga^+ beam with a spot size of about 80 nm (estimated from extrapolation of observed feature sizes with diminishing exposure time). This current corresponds to an ion delivery rate of $6 \times 10^7 \text{ s}^{-1}$, and a dose of order $10^{18} \text{ cm}^{-2} \text{ s}^{-1}$. This dose corresponds to an ion arrival rate of $2 \times 10^3 \text{ s}^{-1}$ per surface atom, assuming a surface density of $5 \times 10^{14} \text{ atoms cm}^{-2}$ on the Si(1 0 0) surface. Steady-state sputter yields for 25 keV Ga^+ normally incident on Si(1 0 0) are about 2 [31], and so the material removal

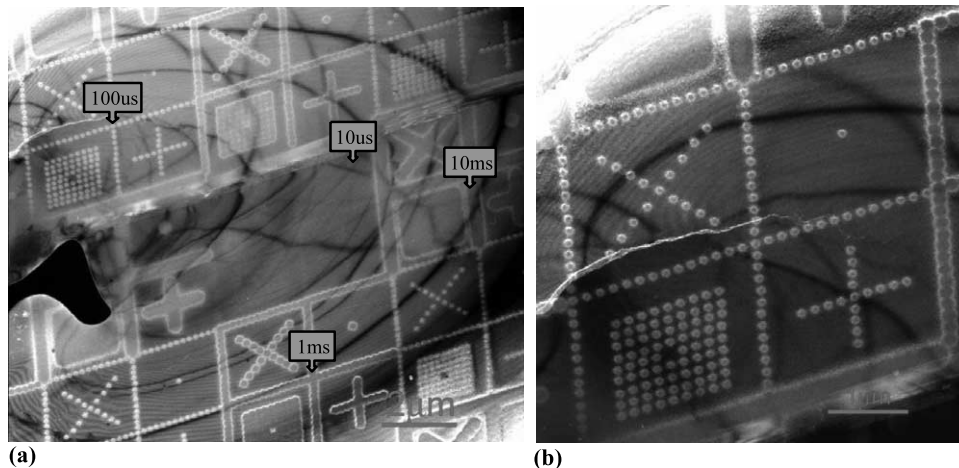


Fig. 1. In situ TEM images ($\langle 2\ 2\ 0 \rangle$ g,3g weak beam) of FIB-fabricated patterns in Si(1 0 0). All patterns were created with a 10 pA Ga⁺ beam. In (a), patterns are shown with different dwell times per feature. In (b), an enlargement of the patterns with a 100 μ s dwell time per feature is shown.

rate on the surface will be about 4×10^3 monolayers per second. Thus, for the enlarged pattern shown in Fig. 1b, corresponding to a feature dwell time of 100 μ s per feature, less than one monolayer of Si is removed. The fact that these features are so clearly visible in the TEM images is a testament to the sensitivity of UHV-TEM imaging to very subtle changes in topography, strain, and crystalline damage.

A fuller description of the observed surface microstructure vs. implantation dose, and the impact upon subsequent Ge nucleation mechanisms will be presented elsewhere [32]. Here, we concentrate on results following 100 μ s Ga⁺ ion beam exposure time per feature, where, as discussed above, monolayer scale topography is produced (as confirmed separately by ex situ AFM scans). The observed feature diameters for this dose are 90 nm (Fig. 2a). Following FIB patterning, the samples are transferred under UHV to the objective lens pole-piece for TEM imaging. The samples are first annealed

to 750 $^{\circ}$ C for 15 min to remove FIB implantation damage. As shown in Fig. 2b, only a few very small (< 6 nm) regions of TEM contrast then remain. This residual contrast could be due to remaining defect clusters or ultra-small dislocation loops, or to γ -Ga precipitates [33]. No remaining surface topography is detectable by ex situ AFM following these scans.

Next, Ge cluster growth is initiated by the introduction of digermane into the sample area at a substrate temperature of 650 $^{\circ}$ C and a digermane partial pressure of 5×10^{-8} Torr. The results are shown in Fig. 3. Over local areas of several square microns, a Ge cluster nucleates on each FIB-patterned feature, and no clusters nucleate between the features. The clusters themselves show considerably different behavior from the behavior

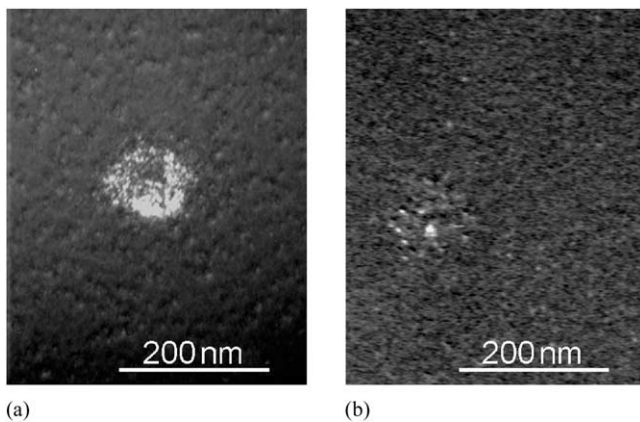


Fig. 2. In situ TEM images ($\langle 2\ 2\ 0 \rangle$ g,3g weak beam) of FIB-fabricated features in Si(1 0 0) at a current of 10 pA and a dwell time of 100 μ s. (a) As implanted and (b) following annealing at 750 $^{\circ}$ C for 15 min.

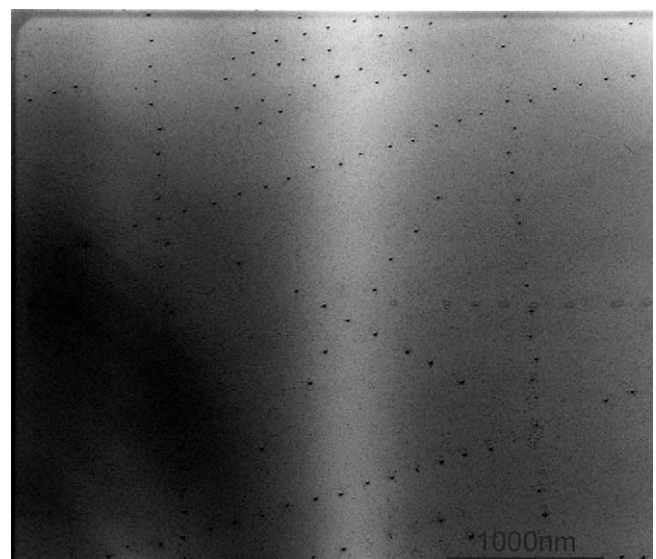


Fig. 3. In situ TEM images ($\langle 2\ 2\ 0 \rangle$ g,3g weak beam) of FIB-fabricated patterns in Si(1 0 0), followed by annealing at 750 $^{\circ}$ C for 15 min and digermane growth at 650 $^{\circ}$ C for 330 s at 5×10^{-8} Torr partial pressure of digermane.

observed on pristine Si(1 0 0) surfaces, as described in Section 2. The aspect ratios of the undislocated clusters, 0.85, are considerably greater than for correspondingly sized islands on unpatterned Si surfaces, of order 0.1. As the islands therefore have considerably more volume at a given diameter, the transition from undislocated to dislocated structures occurs at diameters of 20 nm that are considerably smaller than typical for the unpatterned case (~ 70 nm). It thus appears possible that the residual Ga from FIB sputtering may be acting as a surfactant, modifying surface facet energies and thereby changing aspect ratios and transition volumes/diameters. In any event, this observation produces opportunities for a powerful “demagnifying” effect in cluster dimension and placement. Although the FIB features are 90 nm in diameter, the diameter of the clusters can to a degree be induced to self-terminate at 20 nm because the transition to the dislocated state has a significant energy barrier to the introduction of dislocations. It has previously been observed that for growth on unpatterned Si surfaces, growth of dislocated domes is discontinuous, with growth between dislocation injection events being largely vertical, followed by lateral spurts in growth immediately following each dislocation injection event, leading to “cyclical growth” of such clusters [34]. This is also consistent with the high observed aspect ratio at the dislocation transition in the current work. The placement of the islands is also controlled to better than the patterned feature diameters, given that they form near the center of those features.

As described in Ref. [32], FIB sputtering at substantially greater doses (≥ 1 ms per feature at a 10 pA current) causes substantial surface topography, with Ge cluster nucleation typically observing around the perimeter of the sputtered features.

In summary, it appears clear that FIB pre-patterning of Si(1 0 0) surfaces can accurately guide nucleation of heteroepitaxial Ge clusters, with precision of tens of nanometers. This has been demonstrated at relatively low Ga doses, $< 10^4$ ions per feature, with write speeds of 10^4 features per second. With improved ion optics, placement accuracy and write rates should be further improved.

5. Self-assembly of quantum quadruplets

Under certain $\text{Ge}_x\text{Si}_{1-x}/\text{Si}(1\ 0\ 0)$ growth conditions, we have discovered evolution of a complex surface morphologies that we have termed “quantum quadruplets” and “quantum fortresses” [35] as shown in Fig. 4 for a Ge composition $x = 0.3$, a growth temperature of 550°C , and a growth rate of $0.9\ \text{\AA}\ \text{s}^{-1}$ in the Sandia MBE system. After growth of the Si buffer layer (Fig. 4a), RMS surface roughness is on the monolayer scale.

As the $\text{Ge}_x\text{Si}_{1-x}$ films grow, a characteristic surface pit morphology evolves over film thicknesses of 5–15 nm that we believe to be associated with strain relief mechanisms as proposed by Jesson et al. [36]. The pits have edges along $\langle 0\ 1\ 0 \rangle$ directions, with depths of order 1 nm, widths of approximately 50 nm, and sidewall angles of about 3° at this stage of their evolution. As the film thickness increases to about 15 nm, islands start to form on each edge of the pit perimeters to form a two-dimensional quadruplet (Fig. 4b, inset 1). Further film growth results in the islands forming continuous walls around the pit perimeter by an epitaxial layer thickness of 30 nm (Fig. 4c, inset 2) to form “quantum fortresses”. By now, the pit depth has deepened to about 10 nm, the pit width has doubled to about 100 nm, and the sidewall angle of the pits has increased to 9° (close to the $\langle 5\ 0\ 1 \rangle$ facet angle associated with the hut cluster geometry) [16]. The quantum fortress structures are subsequently destabilized through the introduction of misfit dislocations at 100 nm (Fig. 4d) and at 200 nm (Fig. 4e) epitaxial layer thicknesses.

The quantum quadruplet and fortress morphologies, while entirely reproducible under appropriate growth conditions, are apparently stabilized by conditions that are relatively localized in T, t, ε space. First, it is clear that these structures are strain-stabilized, as the strain disappears due to the introduction of misfit dislocations, so do the quantum fortresses. These configurations are also metastable structures, stabilized only through a relatively narrow range of kinetic pathways. For example, at a composition of $x = 0.3$ and a growth temperature of 550°C , we observe the fortresses at growth rates of 0.9 and $3.0\ \text{\AA}\ \text{s}^{-1}$, but not at $0.15\ \text{\AA}\ \text{s}^{-1}$. These structures are not present at temperature of 650°C for a growth rate of $0.9\ \text{\AA}\ \text{s}^{-1}$. Thus, it is clear that if surface diffusion lengths are high enough, the quadruplet/fortress morphologies do not form (instead we observe the standard hut cluster-like morphologies described in Refs. [16,20]).

These results have been reproduced in an entirely different MBE system at UVa, where we can efficiently map out the conditions for quantum fortress/quadruplet formation by deliberately induced and quantitatively controlled variations in epilayer composition and thickness (essentially determined by the flux distribution from the deposition sources in the absence of substrate rotation). As well as providing more systematic data on the ranges of growth conditions over which these structures form, we can observe transition regions between these structures and more conventional surface morphologies, which reveal fascinating intermediate variants of the fortress morphology. For example in Fig. 5, we observe a characteristic structure that we have observed in several samples, where a quantum fortress appears to be forming a “double wall”. Such structures

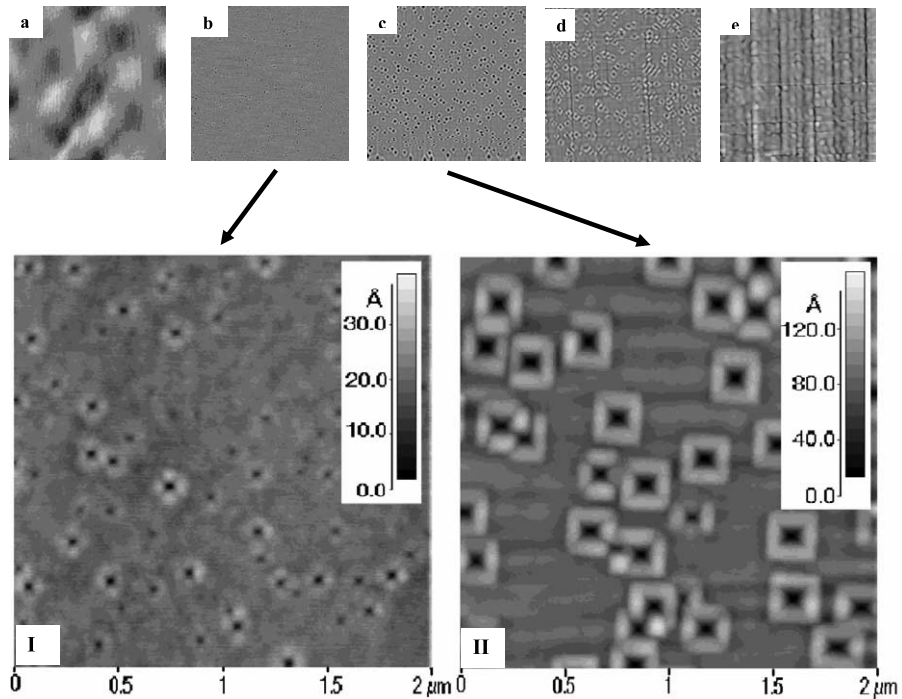


Fig. 4. Evolution of the “quantum fortress” surface morphology for growth of $\text{Ge}_{0.3}\text{Si}_{0.7}/\text{Si}(1\ 0\ 0)$ at a growth temperature of $550\ ^\circ\text{C}$ and a growth rate of $0.9\ \text{\AA}\ \text{s}^{-1}$. AFM scans are $5\ \mu\text{m} \times 5\ \mu\text{m}$ in area. $\text{Ge}_{0.3}\text{Si}_{0.7}$ film thicknesses are (a) 0 nm; (b) 15 nm; (c) 30 nm; (d) 53 nm; (e) 100 nm; and (f) 200 nm.

indicate that there may be a range of stages in the evolution of these morphologies, further study of which will hopefully provide the key to fundamental understanding of the formation and stability of these microstructures.

A similar surface morphology has been previously reported in the $\text{Ge}_x\text{Si}_{1-x}/\text{Si}(1\ 0\ 0)$ system [37]. However, in that work, quantum quadruplets were induced by deliberate incorporation of C, resulting in SiC precipitates that induce pit formation in the Si buffer layer. Subsequent growth of $\text{Ge}_x\text{Si}_{1-x}$ alloy induces

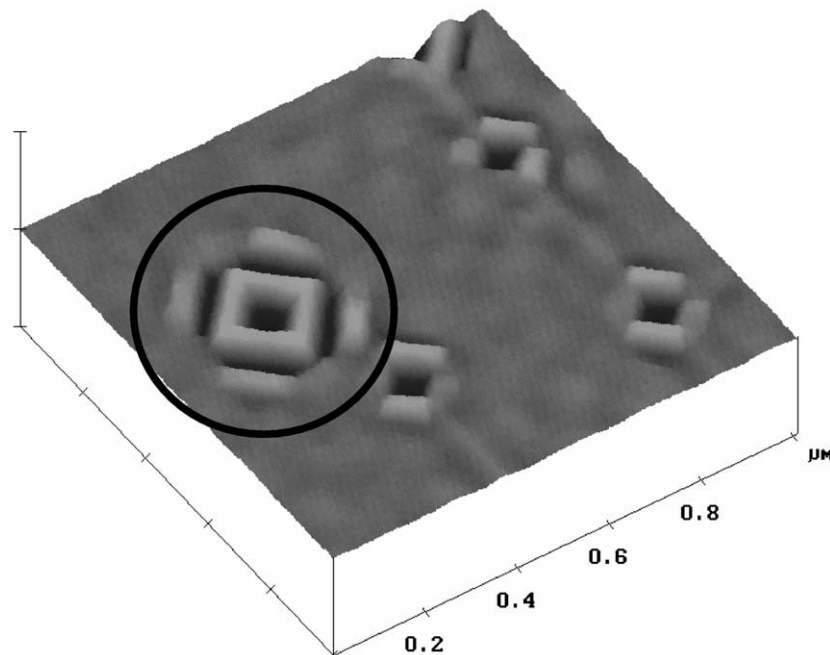


Fig. 5. A $1\ \mu\text{m} \times 1\ \mu\text{m}$ AFM image of a “double-walled” quantum fortress (circled) for 50 nm $\text{Ge}_{0.23}\text{Si}_{0.77}$ films on $\langle 100 \rangle$ Si at a growth temperature of $550\ ^\circ\text{C}$ and a growth rate of $1.0\ \text{\AA}\ \text{s}^{-1}$. Vertical scale of AFM image is 75 nm per division.

cooperative nucleation of quadruplet islands on the pit edges, as observed in this work. In contrast, the quantum fortress morphology in our work appears to be intrinsically associated with the growth conditions and associated kinetically limited strain relaxation pathways.

Finally, we note that the quantum quadruplet morphology has the same symmetry as that required for the concept of QCAs [3,4]. In principle, the location of the initial pits may be programmable by lithographic seeding, and their sizes may be scaleable through epilayer thickness and composition (strain). Initial attempts are being performed to electrically contact these structures, in collaboration with Snider and coworkers at the University of Notre Dame.

6. Conclusions

We have demonstrated in this paper two new methods for assembling complex Ge cluster geometries on Si(1 0 0) surfaces with sub-100 nm precision. In situ FIB implantation can be used to control subsequent Ge cluster nucleation through both chemical and topographical effects. On unpatterned surfaces, quantum dot quadruplets can be spontaneously formed through a novel and complex kinetically controlled pathway for surface microstructural evolution. In this process, square (sidewalls along $\langle 0 1 0 \rangle$), shallow pits first form in the growing heteroepitaxial film as a strain relief mechanism, followed by formation on each pit edge of a Ge cluster to form a “quantum quadruplet” structure. During subsequent heteroepitaxial growth, these islands elongate along the wall edges to form a continuous “quantum fortress” structure. These approaches can be used to control heteroepitaxial cluster nucleation, with potential application to novel nanoelectronic architectures such as QCAs.

Acknowledgements

The authors would like to acknowledge invaluable discussions with G. Snider (Notre Dame University) and R. Tromp (IBM). This work was funded by NSF-DMR through the NSF-MRSEC at UVa, “The Center for Nanoscopic Materials Design” and the UVa-UIUC-IBM-Sandia Focused Research Group “Nanoscale Morphological Evolution of Semiconductor Surfaces” (Grant No. 0075116). J.A.F. was supported by the Division of Materials Science and Engineering, Office of Science, US Department of Energy. Sandia is a multiprogram laboratory operated by Sandia Corporation, a Lockheed Martin Company, for the US Department of Energy under Contract No. DE-AC04-94AL85000.

References

- [1] J. Tersoff, Phys. Rev. Lett. 74 (1995) 4962.
- [2] C. Teichert, M.G. Lagally, L.J. Peticolas, J.C. Bean, J. Tersoff, Phys. Rev. B 53 (1996) 16334.
- [3] G. Bernstein, C. Bazan, M. Chen, C.S. Lent, J.L. Merz, A.O. Orlov, W. Porod, G.L. Snider, P.D. Tougaw, Superlattices Microstruct. 20 (1996) 447.
- [4] G.L. Snider, A.O. Orlov, R.V. Kumamuru, R. Ramasubramanian, I. Amlani, G.H. Bernstein, C.S. Lent, in: E.A. Stach, E.H. Chason, R. Hull, S.D. Bader (Eds.), Mater. Res. Soc. Symp. Proc., Vol. 696, Materials Research Society, Warrendale, PA, 2002, p. 221.
- [5] Y. Nitta, M. Shibata, K. Fujita, M. Ichikawa, Surf. Sci. 462 (2000) L587.
- [6] (a) T.I. Kamins, R.S. Williams, Appl. Phys. Lett. 71 (1997) 1201; (b) T.I. Kamins, D.A.A. Ohlberg, R.S. Williams, W. Zhang, S.Y. Chou, Appl. Phys. Lett. 74 (1999) 1773.
- [7] G. Jin, J. Wan, Y.H. Luo, J.L. Liu, K.L. Wang, J. Cryst. Growth 227–228 (2001) 1100.
- [8] T.I. Kamins, D.A.A. Ohlberg, R.S. Williams, W. Zhang, S.Y. Chou, Appl. Phys. Lett. 74 (1999) 1773.
- [9] T. Ogino, Y. Homma, Y. Kobayashi, H. Hibino, K. Prabhakaran, K. Sumitomo, H. Omi, D. Bottomley, A. Kaneko, F. Ling, Z. Zhang, M.P. Hals, Abstract S-VIII.1, European MRS Meeting, Strasbourg, France, June 2002.
- [10] (a) J.W. Matthews, A.E. Blakeslee, J. Cryst. Growth 27 (1974) 118; (b) J.W. Matthews, A.E. Blakeslee, J. Cryst. Growth 29 (1975) 373; (c) J.W. Matthews, A.E. Blakeslee, J. Cryst. Growth 32 (1976) 265.
- [11] M.L. Green, B.E. Weir, D. Brasen, Y.F. Hsieh, G. Higashi, A. Feyngenson, L.C. Feldman, R.L. Headrick, J. Appl. Phys. 69 (1991) 745.
- [12] D.C. Houghton, C.J. Gibbins, C.G. Tuppen, M.H. Lyons, M.A.G. Halliwell, Appl. Phys. Lett. 56 (1990) 460.
- [13] J.C. Bean, L.C. Feldman, A.T. Fiory, S. Nakahara, I.K. Robinson, J. Vac. Sci. Technol. A 2 (1984) 436.
- [14] R. Hull, J.C. Bean, Crit. Rev. Solid State Mater. Sci. 17 (1992) 507–546.
- [15] D.J. Eaglesham, M. Cerullo, Appl. Phys. Lett. 58 (1991) 2276.
- [16] Y.-W. Mo, D.E. Savage, B.S. Swartzentruber, M.G. Lagally, Phys. Rev. Lett. 65 (1990) 1020.
- [17] M. Tomitori, K. Watanabe, M. Kobayashi, O. Nishikawa, Appl. Surf. Sci. 76/77 (1994) 322.
- [18] F.M. Ross, R.M. Tromp, M.C. Reuter, Science 286 (1999) 1931.
- [19] G. Medeiros-Ribeiro, A.M. Bratkovski, T.I. Kamins, D.A.A. Ohlberg, R.S. Williams, Science 279 (1998) 353.
- [20] J.A. Floro, E. Chason, L.B. Freund, R.D. Twisten, R.Q. Hwang, G.A. Lucadamo, Phys. Rev. B 59 (1999) 1999.
- [21] R.M. Tromp, F.M. Ross, M.C. Reuter, Phys. Rev. Lett. 84 (2000) 4641.
- [22] P. Sutter, M.G. Lagally, Phys. Rev. Lett. 84 (2000) 4637.
- [23] M. Hammar, F.K. LeGoues, J. Tersoff, M.C. Reuter, R.M. Tromp, Surf. Sci. 349 (1995) 129.
- [24] FEI Company, 7451 NW Evergreen Parkway, Hillsboro, OR.
- [25] F.M. Ross, J. Tersoff, M.C. Reuter, F.K. LeGoues, R.M. Tromp, Microsc. Res. Tech. 42 (1998) 281.
- [26] E.A. Stach, R. Hull, R. Tromp, M. Reuter, M. Copel, F. LeGoues, J. Bean, J. Appl. Phys. 83 (1998) 1931.
- [27] J.A. Floro, E. Chason, Mater. Res. Soc. Symp. Proc. 406 (1996) 491.
- [28] J.A. Floro, E. Chason, S.R. Lee, R.D. Twisten, R.Q. Hwang, L.B. Freund, J. Electron. Mater. 26 (1997) 983.

- [29] A. Ishizaka, K. Nakagawa, Y. Shiraki, in: Proceedings of the Second International Symposium on MBE, Jpn. Soc. Appl. Phys., Tokyo, Japan, 1982, pp. 183–186.
- [30] D.A. Glocker, S.I. Shah (Eds.), Handbook of Thin Film Process Technology, Institute of Physics Publishing, Bristol, UK, 1995, pp. E1.0:8 (see, for example).
- [31] (a) J.G. Pellerin, D.P. Griffis, P.E. Russell, J. Vac. Sci. Technol. B 8 (1990) 1990 (see, for example);
(b) C. Lehrer, L. Frey, S. Petersen, H. Ryssel, J. Vac. Sci. Technol. B 19 (2001) 2533 (see, for example).
- [32] M. Kammler, R. Hull, M.C. Reuter, F.M. Ross, Appl. Phys. Lett., in press.
- [33] M. Tanaka, K. Furuya, T. Saito, Nucl. Instrum. Meth. Phys. Res. B 127/128 (1997) 98.
- [34] F.K. LeGoues, M.C. Reuter, J. Tersoff, M. Hammar, R.M. Tromp, Phys. Rev. Lett. 73 (1994) 300.
- [35] J. Gray, R. Hull, J. Floro, Appl. Phys. Lett. 81 (2002) 2445.
- [36] D.E. Jesson, K.M. Chen, S.J. Pennycook, T. Thundat, R.J. Warmack, Phys. Rev. Lett. 77 (1996) 1330.
- [37] X. Deng, M. Krishnamurthy, Phys. Rev. Lett. 81 (1998) 1473.